Submitted to the MRS Conference Proceedings, 1989. CONF-891119--135

2

X-RAY STUDIES OF THE LIQUID/VAPOR INTERFACE: WATER AND POLYMER AND FATTY ACID MONOLAYERS ON WATER

BNL-44872

M. L. Schlossman*, D. K. Schwartz*, E. H. Kawamoto*, G. J. Kellogg*, P. S. Pershan*, B. M. Ocko**, M. W. Kim***, and T. C. Chung***
*Department of Physics and Division of Applied Sciences, Harvard University, Cambridge, MA 02138
**Department of Physics, Brookhaven National Laboratory, Upton, NY 11973
***Exxon Corporate Research Laboratory, Annandale, NJ 08801

BNL--44872
DE90 015680

ABSTRACT

X-ray specular reflectivity is used to study the liquid-vapor interface of pure water and of fatty acid and polymer monolayers at that interface. For the pure water surface the reflectivity was measured for three different spectrometer resolutions and simultaneous fits with only one free parameter to all of the data are in excellent agreement with the prediction of capillary wave theory for the RMS surface roughness. Diffuse scattering away from the specular condition, at wavevectors corresponding to those of the capillary waves, yields intensities and line shapes in agreement with theory with no significant adjustable parameters. Reflectivity from separate monolayers of co-poly 1,2-butadiene/butyl alcohol (50% random substitution) and lignoceric acid ($CH_3(CH_2)_{22}COOH$) at the water/vapor interface are interpreted to obtain profiles of the average electron density $\rho(z)$ as a function of distance z along the surface normal. For the polymer monolayer we find the following: 1) a local maximum in the electron density approximately 10% larger than that of the bulk polymer and 2) the RMS roughness of the vapor/polymer interface agrees with capillary wave theory predictions for the lower surface pressures. For the highest surface pressure the RMS roughness exceeds the value predicted by the capillary wave model. Measurements of reflectivity from a lignoceric acid monolayer, as a function of surface pressure throughout an isotherm (near room temperature), reveal the following behavior: 1) the overall thickness of the monolayer increases with increasing pressure and 2) the head groups occupy a progressively larger region along the surface normal as the pressure increases, indicating that they rearrange normal to the interface.

INTRODUCTION

X-ray specular reflectivity from the liquid/vapor interface is used to investigate the surface structure of water and insoluble monolayers on the water surface. If $d\langle\rho(z)\rangle/dz$ is the derivative (along the direction normal to the surface) of the electron density, $\rho(x,y,z)$, averaged over the plane of the surface, then the ratio of the measured reflectivity, $R(Q_z)$, as a function of the transferred momentum, Q_z, to the theoretical Fresnel reflectivity, $R_F(Q_z)$, from a sharp, flat interface with no structure is given by the approximation [1]:

$$\frac{R(Q_z)}{R_F(Q_z)} = \left| \frac{1}{\rho_{bulk}} \int dz \frac{d\langle\rho(z)\rangle}{dz} \exp(iQ_z z) \right|^2 , \qquad (1)$$

Received by OSTI
AUG 2 0 1990

MASTER

when $Q_z \geq 5Q_c$. The parameter ρ_{bulk} is the electron density far below the surface (in this case, ρ_{water}), $Q_z = |Q_{out} - Q_{in}| = (4\pi/\lambda)\sin\theta$, λ is the x-ray wavelength and θ is measured from the surface plane, *i.e.*, $\theta = 90°$ at normal incidence. Neglecting absorption effects the Fresnel reflectivity, R_F, is given by

$$R_F(Q_z) = \left| \frac{Q_z - \sqrt{Q_z^2 - Q_c^2}}{Q_z + \sqrt{Q_z^2 - Q_c^2}} \right|^2, \tag{2}$$

where the critical wavevector $Q_c \equiv (4\pi/\lambda)\sin(\theta_c) \approx 4\sqrt{\pi\rho_{bulk} r_e}$ ($= 0.0217$ Å^{-1} for water) and $r_e = e^2/mc^2$ is the classical electron radius.

For reflection from the water surface the ratio $R(Q_z)/R_F(Q_z) \approx \exp(-Q_z^2\sigma^2)$ and the electron density gradient can be represented by $(\rho_{bulk}^{-1})\, d\langle\rho(z)\rangle/dz \approx (1/\sqrt{2\pi\sigma^2})\exp(-z^2/2\sigma^2)$. The width σ is dominated by fluctuations in the height of the surface due to thermally excited capillary waves. We will show below that the dependence of the measured σ^2 on the spectrometer resolution agrees with the prediction of the capillary wave model. In addition, off-specular scattering at wavevectors corresponding to those of capillary waves was measured and agrees with the prediction of the capillary wave model. For monolayers on water, the electron density gradient has interfacial widths due to capillary wave fluctuations as well as structure due to packing of the molecules at the interface. The surface pressure and density of the molecules in the monolayer are varied and the resultant changes in the electron density profile are measured.

Experimental details common to all the samples will be discussed first. The three systems, i.e., the pure water liquid/vapor interface, the monolayer of co-poly 1,2-butadiene/butyl alcohol (50% random substitution) (PBBA), and the monolayer of lignoceric acid are then individually discussed.

EXPERIMENTAL

A solid teflon Langmuir trough enclosed in a sealed Aluminum box was used to hold the Millipore Milli-Q [2] water used as the sample or as the subphase for the monolayers. Water can be added and removed and its surface aspirated (to remove impurities) without opening the box. The box was flooded with high-purity nitrogen gas and temperature controlled to within 0.1 K. A filter paper [3] Wilhelmy plate was used to measure the surface tension *in situ* with a resolution of 0.01 dynes/cm and an accuracy of ±0.5 dynes/cm (this large variation is due to buoyant displacement of the plate for different water levels). The surface pressure, π, is the deviation of the surface tension, γ, from the measured value for pure water, $\pi = \gamma_{water} - \gamma$. The surface purity of the water can be evaluated *in situ* by measuring the change in surface tension that accompanies the sweep of a teflon barrier across the surface. Typically, the surface was taken to be clean when the surface tension changed by less than 0.05 dynes/cm for an area compression by a factor of 4. A pure water surface can be kept clean, by this criterion, for 24 hours.

The experiments were performed on beam line X22B at the National Synchrotron Light Source (NSLS) at Brookhaven National Laboratory using a liquid surface reflectometer that has been described elsewhere [1]. For specular reflection from the pure water surface and the polymer monolayer, the x-ray wavelength λ=1.2569±0.0002Å, and for diffuse scattering from the pure water surface and specular reflection from the fatty acid monolayer, λ = 1.3965±0.0002Å. A Ge (111) monochromator was used to deflect the beam downward by an angle α onto the sample. The size of the incident beam was defined by a slit (approximately 400 mm from the monochromator) with dimensions $h_i x w_i$ (height by width), where $h_i \cong 0.2$ mm and $w_i \cong 3\text{-}4$ mm. The distance L from the monochromator to the sample and from sample to detector was approximately 600 mm. The measured angular spread was $\Delta\alpha \equiv 6 \times 10^{-5}$ radians in the vertical and $\Delta\Phi \equiv 1 \times 10^{-3}$ radians in the horizontal. The magnitude of h_i was chosen so that all of the incident beam reflected off the sample. The detector slit was positioned so the detector accepted radiation at an angle β from the horizontal and at an azimuthal angle ϕ. The wavevector transfer is given by $\mathbf{Q} = \mathbf{Q}_{out} - \mathbf{Q}_{in}$: $Q_z = (2\pi/\lambda)\,[\sin(\alpha) + \sin(\beta)]$, $Q_x = (2\pi/\lambda)\sin(\phi/2)\,[\cos(\beta) + \cos(\alpha)]$, and $Q_y = (2\pi/\lambda)\cos(\phi/2)\,[\cos(\beta) - \cos(\alpha)]$. The specular condition $\alpha=\beta\equiv\theta$ and $\phi=0$ is equivalent to $Q_x = Q_y = 0$. The full widths at half maximum of the vertical and horizontal angular spread accepted by the detector are $\Delta\beta = h_d/L$ and $\Delta\phi = w_d/L$, where h_d and w_d are the height and width of the detector slit.

WATER [4]

In Fig. 1a, reflectivity data normalized to $R_F(Q_z)$ is plotted as $[R(Q_z)/R_F(Q_z)]$ vs. Q_z^2 for three different spectrometer resolutions (three different detector slit heights, h_d = 0.8, 2, and 5 mm). For each resolution the data can be represented by the form, $[R(Q_z)/R_F(Q_z)] = \exp(-Q_z^2\sigma^2)$, where the width σ varies logarithmically with both Q_z and the height of the detector slit. The interfacial width has previously been represented [5] as a combination of a local microscopic electron density gradient σ_o and the capillary wave contribution,

$$\sigma^2 = \sigma_o^2 + \frac{k_BT}{4\pi^2\gamma}\int_{A_s}\frac{dq}{q^2+k_g^2}\ , \qquad (3)$$

where k_BT is the Boltzmann constant times the temperature, γ is the macroscopic surface tension (for water, measured to be 72.5 ± 0.4 dynes/cm), $k_g^2 = \rho_m g/\gamma$ where ρ_m is the *mass* density and g is the gravitational acceleration, and A_s is a circular region with a rectangular cutout in reciprocal space. The inner boundary of A_s is determined by the known resolution of the x-ray reflectometer such that x-rays scattered by capillary waves with wavevectors **q** outside of the inner boundary, and thus contained in A_s, are deflected outside the angular acceptance of a detector centered on the position for specular reflection [6]. Since long wavelength capillary waves scatter at small angles, i.e., within the rectangular cutout of A_s, the σ^2 measured by a detector with finite resolution is not affected by waves at small **q**. Consequently σ^2 is specified in terms of only two adjustable parameters: the intrinsic width of the electron density profile σ_0 and the radius q_{max} of the outer perimeter of A_s.

For these measurements capillary waves with wavelengths of the order of 400 Å to 80,000 Å contribute to the width σ [4]. Since the origin of both σ_0 and q_{max} are microscopic (on the scale of angstroms) they cannot be distinguished by these measurements. The three data sets in Fig. 1a were simultaneously fit to the capillary wave model, with $\sigma_0 = 0$, varying only q_{max}. The solid lines in Fig. 1a represent this fit with $q_{max} = (\pi/1.4 \pm 0.1 Å)$ and $\chi^2 = 1.03$. The inset to Fig. 1a displays values of $\sigma(Q_z)$ derived from the fit and calculated from the theory for $Q_z = 0.4 Å^{-1}$.

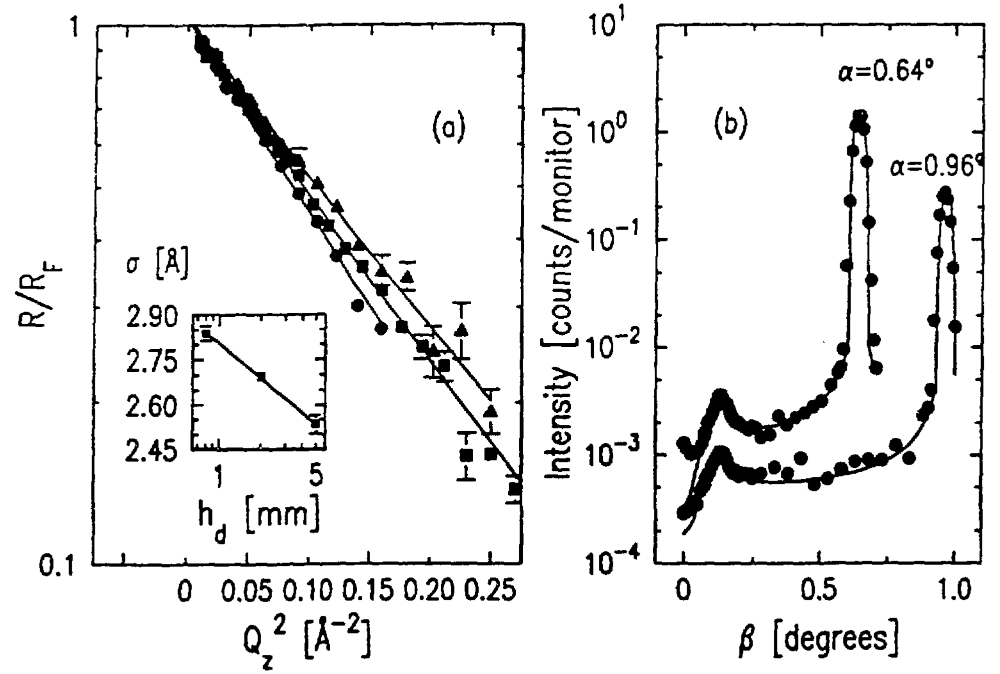

Fig. 1: (a) Specular reflectivity data in the form of $[R(Q_z)/R_F(Q_z)]$ vs. Q_z^2 for detector slit heights of 0.8 mm (•), 2.0 mm (squares), and 5.0 mm (triangles). The solid lines represent the best fit of the model discussed in the text. The inset shows the width of the surface profile plotted vs. the detector slit height. The squares are derived from the fits to the data and the line is calculated from the theory at $Q_z = 0.4 Å^{-1}$.

(b) Scattered intensity, in the plane of incidence, as a function of detector angle β for incident angles $\alpha = 0.64°$ and $0.96°$. The peaks at $\beta = \theta_c \cong 0.13°$ are due to the surface scattering enhancement factor, the peaks at $\beta = \alpha$ are the specular reflectivity signals. The solid line is the theoretical prediction calculated with *no significant adjustable parameters.*

In this model the reduction of $R(Q_z)/R_F(Q_z)$ to less than one occurs due to scattering by capillary waves. To examine this diffuse scattering, x-ray intensity was measured as a function of the outgoing angle β for two fixed incident angles, α, and for $\phi = 0$ (see Fig. 1b). When β is equal to the critical angle for total external reflection, θ_c, the surface field enhancement [7] creates a peak in the scattered intensity. The amplitude and shape of this peak and its tails are sensitive to the scattering cross section from the capillary waves. The scattered intensity, I_D, is written as

$$I_D = I_o \frac{(r_e\rho)^2}{\alpha\,\Delta\alpha} \frac{k_BT}{\gamma} \int_{(\alpha-\Delta\alpha/2)}^{(\alpha+\Delta\alpha/2)} d\alpha \int_{(-\Delta\phi/2)}^{(\Delta\phi/2)} d\phi \int_{(\beta-\Delta\beta/2)}^{(\beta+\Delta\beta/2)} d\beta \, \frac{T(\alpha)\,T(\beta)}{q^2+k_g^2} \quad , \tag{4}$$

where I_o is the total incident flux, r_e is the classical electron radius, $T(\alpha)$ and $T(\beta)$ are the Fresnel surface scattering enhancement factors, $T(\beta) \approx (2\beta/\theta_c)^2\sqrt{R_F(\beta)}$, and $\Delta\alpha$, $\Delta\beta$, and $\Delta\phi$ are the widths of the distributions of the respective angles [8]. The displayed fits in Fig. 1b include a small constant background on the order of 10% of the intensity of the peak at $\beta=\theta_c$.

The agreement between theory and experiment for both the resolution dependence of σ^2 for the specular reflection and for the amplitude and line shape of the diffuse scattering demonstrates that the capillary wave model is a good representation of the height-height correlation function over a region in reciprocal space. This region can be shown [4] to correspond to capillary waves with wavelengths from 400 to 80,000 Å and extends the region (microns to millimeters) previously explored by optical light scattering [9]. Similar measurements can now be made on complex liquid surfaces with confidence that excess diffuse scattering or decreased reflectivity, beyond that expected from thermally excited capillary waves, can be interpreted in terms of other microscopic models.

POLYMER MONOLAYER [10]

Addition of a monolayer of PBBA to the water/vapor interface lowers the surface tension by up to 30%. This section discusses the change in surface structure accompanying this effect. Preparation of PBBA with 1300 monomers was previously described [11]. The polymer was dissolved in methanol and delivered to the surface at an initial surface density of 14 Å^2/monomer. Slow compression over several hours produced the isotherm shown in Fig. 2a. The monolayer can be compressed and expanded with reproducibility of the surface pressure to within $\Delta\pi \leq 0.2 - 0.5$ dynes/cm. For three surface pressures (20.3, 26.8, and 28.2 dynes/cm) in the high density region, the reflectivity data is plotted as $[R(Q_z)/R_F(Q_z)]$ vs. Q_z^2 in Fig. 2b.

Although measured reflectivity for a range of Q_z is typically analyzed by proposing a real space model for the electron density, $\rho(z)$, and using equation (1) to fit the data, in the present case both the roughness of the vapor/polymer interface and the qualitative behavior of the electron density of the monolayer can be understood independent of any model. The following two aspects of the data allow qualitative features of the electron density profile to be determined: 1) for large Q_z, $\log_e[R(Q_z)/R_F(Q_z)]$ decreases linearly with Q_z^2 and is well represented by the form $R(Q_z)/R_F(Q_z) = A^2 \exp(-Q_z^2\sigma^2)$ and 2) for all three data sets, extrapolation of the linear dependence back to $Q_z = 0$ rises above 1, indicating values of $A^2 \cong 1.2$. These aspects indicate that the vapor/polymer

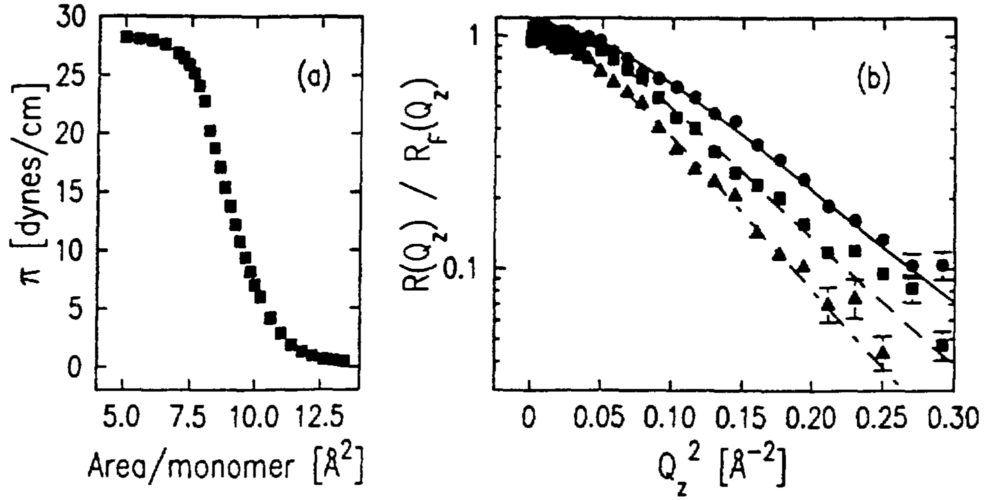

Fig. 2: (a) Isotherm for a monolayer of co-poly 1,2-butadiene/butyl alcohol (50% random substitution) at 20 °C. The surface pressure, π, saturates in the high density region (low surface area/monomer).

(b) The measured $[R(Q_z)/R_F(Q_z)]$ vs. Q_z^2 (symbols) and fits to the model discussed in the text (lines) for three surface pressures: 20.3 (•, solid line), 26.8 (squares, dashed line), and 28.2 (triangles, long-short dashed line) dynes/cm.

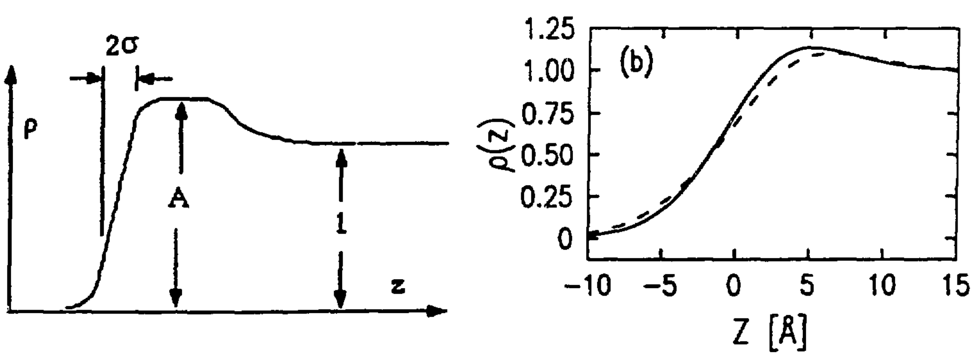

Fig. 3: (a) Schematic illustration of a possible electron density profile consistent with the data in Fig. 2. The gradual decay from $\langle\rho(z)\rangle/\rho_{bulk} \cong A$ to 1 is not necessarily monotonic.

(b) The real space profiles for the two surface pressures, 20.3 (solid line) and 28.2 (dashed line) dynes/cm. The value of z was adjusted by 1 Å for π = 28.2 dynes/cm so $\langle\rho(z)\rangle = 0.5$ at the same z for both pressures (for viewing purposes only).

interface is the sharpest feature of the interfacial profile and that $A > 1$, which implies that the electron density change associated with the sharp step is larger than the change from vapor to bulk water [9]. The only type of reasonable profile satisfying these conditions is illustrated in Fig. 3a. This indicates that the surface electron density exceeds the value for bulk water. Although the density of this polymer in the bulk is not known it can be compared with that of the similar polymer, pure 1,2 polybutadiene [12]. Since the bulk electron density of 1,2 polybutadiene is 0.96 ρ_{water}, the measured peak value of 1.1 ρ_{water} is a surprising result.

A linear fit to the large Q_z region yields a value for the microscopic width, σ, of the polymer/vapor interface that can be compared with the width derived from the capillary wave model. The results for measurements with the same spectrometer resolution are displayed in Table I. For the two lowest pressures the experimental and predicted widths agree, however, *for the highest pressure* the measured width is significantly larger than the capillary wave model prediction. One possible origin for this effect could be buckling of the monolayer, however, any molecular rearrangement that either (i) made the surface locally more diffuse or (ii) made the surface rougher on a length scale that was small in comparison with our in-plane resolution of ~500Å would result in the discrepancy.

Table I: Numerical results for surface polymer monolayer on H_2O. The absolute error in the surface pressure π is ±0.5 dyne/cm, however relative errors are ±0.01 dyne/cm. The value of $\pi = 0$ corresponds to the pure water surface. The width σ is obtained from the slope of $\log_e[R(Q_z)/R_F(Q_z)]$ versus Q_z^2 at large Q_z. The values for σ (capillary theory) were calculated using the same maximum radius for A_s as used for water. The χ^2 values are for the non-linear least squares fits which determine ρ_{max}/ρ_{bulk} and σ_G.

π (surface pressure) (dynes/cm)	σ (vapor/ monolayer) (Å)	σ (capillary theory) (Å)	ρ_{max}/ρ_{bulk}	σ_G (gaussian) (Å)	χ^2
0	2.7 ± 0.01	2.7	--	--	--
20.3	3.18 ± 0.07	3.19	1.13 ± 0.02	4.5 ± 0.25	5
26.8	3.37 ± 0.07	3.41	1.13 ± 0.02	5.0 ± 0.25	2.4
28.2	3.71 ± 0.07	3.41	1.08 ± 0.02	5.0 ± 0.25	3.2

The qualitative features indicated in Fig. 3a are a guide to the choice of a real space profile. A more quantitative view of the monolayer can be obtained by fitting the data to a real space model for $\rho(z)$, such as

$$\frac{\langle\rho(z)\rangle}{\rho_{water}} = \frac{1}{2}\left[1 + \mathrm{erf}\left(\frac{z}{\sigma\sqrt{2}}\right)\right] + B\exp\left(\frac{-(z-z_0)^2}{2\sigma_G^2}\right), \qquad (5)$$

where, in the first term, $\mathrm{erf}(z/\sigma\sqrt{2})$ is an error function of width σ describing the vapor/polymer interface. The second term, which models the extra electron density of the polymer beyond that of the water, is a gaussian of amplitude B and width σ_G that is offset from the vapor/polymer interface by the distance z_0. This model was used to fit the data for $Q_z \geq 0.1$ Å$^{-1} \equiv 5Q_c$, the region in which the Born approximation leading to Eq. (1) is very accurate. The vapor/polymer interface width, σ, was held constant at the value obtained from the separate fit (as previously discussed) in the large Q_z region. Two of the parameters, B and z_0, are strongly correlated and can be reparametrized by the quantity, ρ_{max}/ρ_{bulk}, where ρ_{max} is the local maximum of the electron density and represents an overall amplitude for the monolayer. The two free parameters, ρ_{max}/ρ_{bulk} and σ_G, are tabulated in Table I. The values and their error bars were derived by mapping the χ^2 - parameter space. Fits to the data are shown in Fig. 2b and the real space $<\rho(z)>/\rho_{water}$ is shown in Fig 3b (for only two pressures for visual clarity). The maximum electron density is typically 10% greater than the water density and its position moves further from the vapor/polymer interface as the pressure increases. The monolayer remains quite thin ($2\sigma_G \approx 10$ Å) even at these very high pressures. The peak electron density for the highest pressure is slightly less than for the lower pressures, as would be expected for an interface that may have buckled or otherwise rearranged itself normal to the interface.

LIGNOCERIC ACID MONOLAYERS [13]

Monolayers at the water/vapor interface of lignoceric acid ($CH_3(CH_2)_{22}COOH$), a long chain fatty acid [14] that is electrically neutral on a pH = 2 substrate (water and HCl) are studied. The surface pressure was allowed to fully relax for each surface density on the isotherm. Measurement of an equilibrium isotherm in this manner may take up to 24 hours. The isotherms measured simultaneously with x-ray reflectivity scans are shown in Fig. 4a. The isotherm has one flat region typical of a coexistence region. Five reflectivity scans, from several isotherms (for the temperature range, 19.7 ± 0.2 °C), specified by the surface pressure are shown in Fig. 4b. The qualitative features of minima and maxima indicate destructive and constructive interference between x-rays reflected from different interfaces within the electron density profile. The trend of the minima to move towards smaller Q_z for higher surface pressures indicates that the monolayer thickens as the pressure increases. More detailed features of the monolayer can be derived by proposing an electron density profile for the interface.

The electron density profile illustrated in Fig. 5a was used to fit the data in Fig. 4b. The profile can be written as

$$\frac{<\rho(z)>}{\rho_w} = \frac{\rho_t}{2\rho_w}\left[1+\mathrm{erf}\left(\frac{z}{\sqrt{2\sigma^2}}\right)\right] + \frac{1-(\rho_t/\rho_w)}{2}\left[1+\mathrm{erf}\left(\frac{z-(D-z_0)}{\sqrt{2\sigma_2^2}}\right)\right]$$

$$+\frac{A_G}{\sqrt{2\pi\sigma_G^2}}\exp\left[\frac{-(z-D)^2}{2\sigma_G^2}\right]. \qquad (6)$$

The first term describes the interface between the vapor and the hydrocarbon tail region ($CH_3(CH_2)_{22}$ -) of the monolayer where ρ_t is the electron density of the tail,

ρ_w is the electron density of the bulk water, and σ is the RMS interfacial

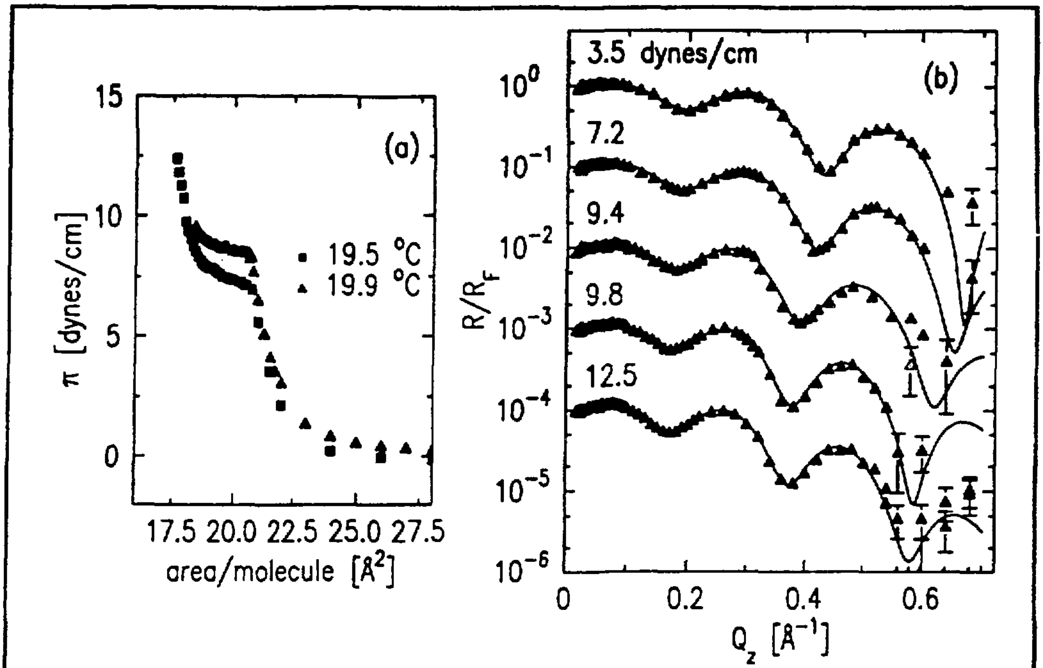

Fig. 4: (a) Isotherms for lignoceric acid measured simultaneously with reflectivity scans at 19.5 °C (squares) and 19.9 °C (triangles).
(b) Measured $[R(Q_z)/R_F(Q_z)]$ for different surface pressures. The solid lines correspond to fits to a model electron density discussed in the text.

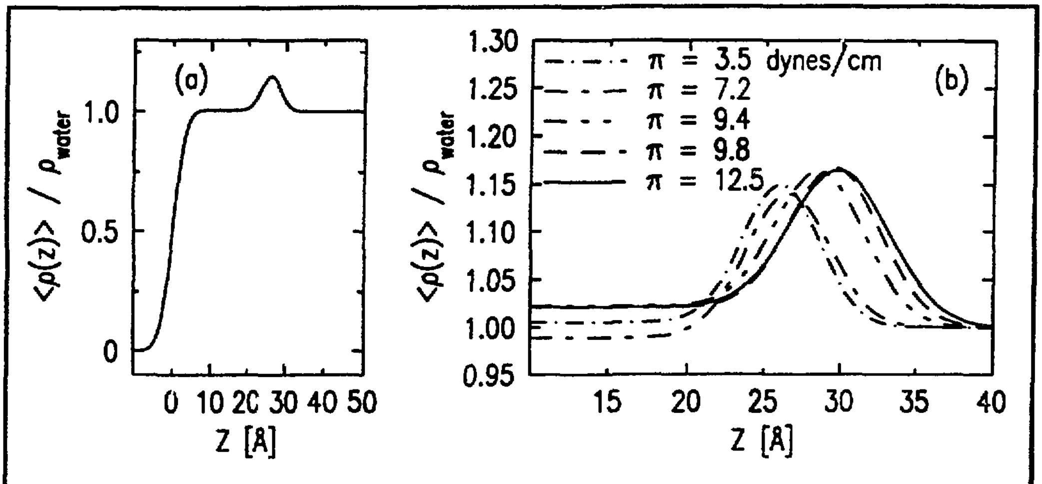

Fig. 5: (a) An illustration of the electron density profile used to fit the data in Fig. 4b. (b) Detail of the head group region from the fit to the data sets in Fig. 4b. The vapor/tail interface (not shown) is located at z=0.

width. The third term is a gaussian describing the excess electron density due to the head group (the carboxyl group COOH) where A_G is the area under the gaussian, σ_G is the gaussian width and D is the distance from the vapor/tail interface to the center of the gaussian. D is a measure of the thickness of the monolayer. The second term represents a transition region which allows the water and the tail regions to have different electron densities. The parameter σ_2 is the width of this transition and z_0 is the distance offset from the gaussian head group. For this set of data, the second term plays a negligible role because $(\rho_t/\rho_w) = 1\pm0.02$ (this value is derived from the fitting).

The results of fitting this model for $\langle\rho(z)\rangle$ are shown as lines in Fig. 4b and are tabulated in Table II. A detail of $\langle\rho(z)\rangle$ for the head group region is shown in Fig. 5b. The position of the head group corresponds to the thickness of the monolayer, D, which increases from 26.1Å to 30.1Å as the surface pressure increases from 3.5 to 12.5 dynes/cm. The thickness changes only slightly when the monolayer passes through the kink in the isotherm or throughout part of the flat region, however, it changes dramatically as the steep rise in the high density region is approached. The thickness can be interpreted in terms of a molecular tilt angle, θ_t, from the surface normal if a particular molecular conformation is assumed. An all trans conformation for the C-C bonds would result in a molecular length of 29.25 Å for the tail and an additional 0.5Å to the center of the head group. The tilts listed in Table II are calculated from this rigid chain model. The molecular tilt changes from 30° to approximately 0°. The change occurs during the approach to the high density region. The existence of some gauche bonds cannot be excluded by this data and the chains may not be as long as the all-trans length. Further information about this structure may be obtained from recent surface scattering studies on the in-plane structure of this or similar monolayers [13,15]. Glancing incidence Bragg diffraction from 2-d crystalline domains has been seen throughout the isotherm, *including the lower density region* below the kink. The Bragg peaks, at present, are resolution limited and indicate crystalline sizes of at least several hundred angstroms.

Table II: Numerical results for lignoceric acid monolayer on H_2O. The absolute error in the surface pressure π is ±0.5 dyne/cm, however, relative errors are ±0.01 dyne/cm. The absolute error in the temperature is ± 0.5 °C, however, relative errors are ± 0.1 °C. For the calculated θ_t see the explanation in the text.

π surface pressure (dynes/cm)	surface area/ molecule (Å^2)	temper-ature °C	D ~monolayer thickness (±0.1 Å)	θ_t tilt calculated	σ_G head group width (± 0.1)
3.5	22.2	19.7	26.1	29 ± 2	2.54
7.2	20.2	19.5	26.5	27 ± 2	2.77
9.4	18.4	19.9	28.8	14 ± 3	2.93
9.8	18	19.5	29.8	0 → 5	2.98
12.5	17.6	19.5	30.1	0 → 5	3.26

Two interesting aspects of the head group structure can be extracted. The first is the excess number of electrons associated with the head group. The excess is the number of electrons due to the excess electron density above that of the surrounding regions (water and tail group). In this model the excess is directly related to the area of the gaussian piece of $\langle\rho(z)\rangle$. An unambiguous determination of the total number of electrons in the head group would require reflectivity taken at much larger values of Q_z ($Q_z \approx 0.6$ Å^{-1}). The excess number of electrons for all the data sets is 7 ± 0.1, which is the value calculated from the expected electron densities of the head group and surrounding regions. The constancy of this number implies that the chemical structure of the head group is unchanged throughout the isotherm, as expected. It also indicates the potential of the reflectivity measurement to detect small changes in the chemical structure of the head group.

The second and most striking determination from these reflectivity scans is the width associated with the head group region. This width is not the size of a single molecular head group, but corresponds to the width of the region occupied by the head groups along the surface normal. As listed in Table II and shown in Fig. 5b the head group width increases significantly as the surface pressure increases. This implies interdigitation or some other movement along the surface normal of the head groups relative to each other. The head groups rearrange in response to packing constraints at the surface.

SUMMARY

We have presented results of both specular reflection and diffuse scattering of x-rays from the water surface which can be extended to a systematic study of monolayers at that surface. Two examples were presented of specular reflection studies from a polymer and a fatty acid monolayer. Except for the highest pressure, the polymer/vapor interfacial width agreed with the capillary wave model prediction. The polymer monolayer had an electron density greater than a chemically similar bulk polymer and remained very thin, even at high surface pressures. The fatty acid monolayer exhibited structural rearrangements as a function of surface pressure. The overall thickness of the monolayer increased with increasing pressure. One striking observation is that, for increasing pressure, the head groups occupy a progressively larger region along the surface normal, indicating that they rearrange normal to the interface.

ACKNOWLEDGEMENTS

This work was supported by the National Science Foundation through grants to the Harvard Materials Research Laboratory, NSF-DMR-88-12855 and NSF-DMR-86-14003. Research carried out at the NSLS, Brookhaven National Laboratory, is supported by the Department of Energy, Material Sciences and Division of Chemical Sciences under contract DE-AC02-76CH00016.

---

[1]P. S. Pershan, in *International Conference on Surface and Thin Film Studies Using Glancing-Incidence X-ray and Neutron Scattering*, to be published in J. de Phys. (Paris) (1990), and J. Als-Nielsen, in *Structure and Dynamics of Surfaces*, vol. 2 ch. 4, eds. W. Schammers and P. Blanckenhagen, *Topics in Current Physics*, Springer (1986).

[2]Millipore Corp. Bedford, MA 01730.

[3]Millipore Corp. Bedford, MA 01730. Filter type GS, pore size of 0.22 microns.

[4]D. K. Schwartz, M. L. Schlossman, E. H. Kawamoto, G. J. Kellogg, P. S. Pershan and B. M. Ocko, "Thermal Diffuse X-ray Scattering Studies of the Water-Vapor Interface" (to be published).

[5]A. Braslau, P. S. Pershan, G. Swislow, B. M. Ocko, J. Als-Nielsen, Phys. Rev. A **38**, 2457 (1988) and A. Braslau, M. Deutsch, P. S. Pershan, A. H. Weiss, J. Als-Nielsen, and J. Bohr, Phys. Rev. Lett. **54**, 114 (1985).

[6]The outer boundary of A_s is defined by an upper cutoff similar to that of the Debye heat capacity theory.

[7]R. S. Becker, J. A. Golovchenko, and J. R. Patel, Phys. Rev. Lett. **50**, 153 (1983).

[8]We have chosen a constant, or square wave, angular intensity distribution. This is a good approximation in this case, however, the results are almost identical for a trapezoidal distribution suggesting that they are insensitive to the exact form of the distribution.

[9]R. Loudon, in *Surface Excitations*, edited by V. M. Agranovich and R. Loudon (Elsevier Science Publisher, 1984), chapter 6.

[10]M. L. Schlossman, D. K. Schwartz, E. H. Kawamoto, G. J. Kellogg, P. S. Pershan, M. W. Kim, and T. C. Chung, "X-Ray Reflectivity of a Polymer Monolayer at the Water/Vapor Interface" (to be published).

[11]Mahn Won Kim and T. C. Chung, J. Coll. Int. Sci. **124**, 365 (1988).

[12]Giulio Nutta, Science **147**, 261 (1965).

[13]M. L. Schlossman, D. K. Schwartz, G. J. Kellogg, E. H. Kawamoto, and P. S. Pershan (to be published).

[14]George L. Gaines Jr., *Insoluble Monolayers at Liquid-Gas Interfaces* (Interscience Publisheers, John Wiley and Sons, New York, 1966).

[15]a) K. Kjaer, J. Als-Nielsen, C. A. Helm, P. Tippman-Krayer, and H. Mohwald, J. Phys. Chem. **93**, 3200 (1989), b)P. Dutta, J. B. Peng, B. Lin, J. B. Ketterson, M. Prakash, P. Georgopoulos, and S. Ehrlich, Phys. Rev. Lett. **58**, 2228 (1987), c) S. W. Barton, B. N. Thomas, E. B. Flam, Stuart A. Rice, B. Lin, J. B. Peng, J. B. Ketterson, and P. Dutta, J. Chem. Phys. **89**, 2257 (1988).